The Journal of Immunology, 2026, 215(3), vkag052
https://doi.org/10.1093/jimmun/vkag052
Research Article

Effectiveness and immunogenicity of a nanoemulsion protein subunit vaccine against *Pseudomonas aeruginosa*: investigation in diet-induced obese mice

Satabdi Biswas[1,2], Debaki Ranjan Howlader[1,2], Zackary Dietz[1,2], Prolay Halder[1,2], Suhrid Maiti[1,2], Ti Lu[1,2], Robert K. Ernst[3], William D. Picking[1,2], and Wendy L. Picking[1,2,*]

[1]Department of Veterinary Pathobiology and Integrative Biomedical Sciences, University of Missouri, Columbia, MO 65201, United States
[2]Bond Life Sciences Center, University of Missouri, Columbia, MO 65201, United States
[3]Department of Microbial Pathogenesis, University of Maryland, Baltimore, MD 21201, United States
*Corresponding author: Email: wendy.picking@missouri.edu

Abstract

***Pseudomonas aeruginosa* (Pa) is an opportunistic pathogen threatening individuals with obesity, a condition associated with chronic meta-inflammation and altered immunity. In this study, we evaluate the immunogenicity and protective efficacy of a nanoemulsion-based subunit vaccine (L-PaF/ME/BECC) targeting Pa in a diet-induced obese mouse model. Mice fed a high-fat diet (HFD; 60% fat) were compared to those on a low-fat diet (LFD; 10% fat) or regular chow (3% to 4% fat) to assess differences in vaccine responsiveness. Our results show that while L-PaF induces robust immune responses across all groups, HFD-fed mice exhibit significantly impaired antibody quality, including reduced IgA, IgG1, and IgG3 titers. These deficiencies were associated with impaired germinal center B-cell and T follicular helper cell responses, along with reduced CXCR5 and PD-1 modulation. In contrast, LFD-fed mice displayed preserved germinal center architecture and enhanced class-switched antibody production. This immune impairment extended to the lung-resident memory B cell in HFD mice, whereas LFD mice maintained a functional response. Despite compromised humoral immunity, HFD mice showed an expansion of lung tissue-resident memory T (Trm) cells postvaccination. FTY720 treatment showed that early secondary protection against Pa was maintained in the absence of circulating T-cell recruitment, consistent with a dominant contribution of lung-resident immune mechanisms during this early recall phase. Together, these findings suggest that lung Trm-associated immunity may partially compensate for obesity-associated defects in humoral responses and highlight the importance of vaccine strategies that promote tissue-localized T-cell immunity in metabolically compromised hosts.**

Keywords obesity, *Pseudomonas aeruginosa*, resident memory, subunit vaccine, T3SS

Introduction

Obesity is a chronic and complex disease with an accumulation of excessive visceral fat, resulting in a high body mass index (>30 kg/m^2). Obesity rates have surged 3-fold since 1975,[1] with 33% of adults and 17% of children being classified as obese or overweight in the United States.[1] The accumulated metabolically active visceral fat contributes to "meta-inflammation," which exacerbates inflammatory responses that may be triggered by an infection.[2,3] Meta-inflammation results in sustained activation of macrophages, which in turn promote the release of proinflammatory cytokines, including TNF-α, IL-6, and IL-1β, and others. Despite producing more proinflammatory cytokines, people with obesity tend to experience more severe viral and bacterial pneumonia.[4–6] Obesity was thus identified as a major risk factor for respiratory virus infection–related deaths during the coronavirus disease 2019 (COVID-19)[6] and 2009 influenza A (H1N1)[7] pandemics.

The "double pandemic," referring to the synergistic interplay between obesity and infection, is evident in both viral and bacterial diseases.[8] In particular, obesity-related impairment of pulmonary host defenses increases susceptibility to infections caused by the opportunistic gram-negative pathogen *Pseudomonas aeruginosa* (Pa).[9] Pa is a leading cause of severe pneumonia, particularly in individuals with weakened immune systems.[9,10] A recent study has shown obesity to elevate the severity of Pa-pneumonia through decreased phagocytosis via alveolar macrophages (AMs).[4] Moreover, the innate and emerging antibiotic resistance of Pa has made these infections increasingly difficult to treat. Multidrug-resistant (MDR) strains of Pa are now recognized by

Received: September 4, 2025. **Revised:** February 7, 2026. **Accepted:** February 10, 2026

health authorities as critical threats due to their limited treatment options.[11] Globally, these infections contribute significantly to the healthcare burden.[12,13] According to the 2019 Centers for Disease Control and Prevention Antibiotic Resistance Threats report, MDR Pa poses a severe risk with approximately 32,600 hospitalized individuals contracting MDR Pa in 2017, resulting in 2,700 deaths and $757 million in medical costs in the United States.[14] A further escalation of these Pa infections then continued from 2019 to 2022.[14] Given the existing literature highlighting the impaired bacterial clearance in high-risk populations, the development of effective prophylactic measures is imperative to combat the escalating issue of antibiotic resistance in Pa.

Vaccination stands as one of the greatest public health achievements of our time, playing a crucial role in controlling past and present epidemics and pandemics.[15,16] Previous studies on COVID-19 and influenza suggest that obese individuals face a higher risk of severe outcomes, including death, which is directly linked with reduced neutralizing antibody titers.[17–19] Furthermore, the reduced efficacy of hepatitis B and rabies vaccines has been linked to lower antibody levels in obese populations.[20,21] However, unlike vaccines against viral pathogens, no studies have yet examined the effectiveness of vaccines targeting gram-negative bacterial pathogens in obese individuals. Given the high burden of Pa infections in immunocompromised and at-risk populations, we considered it was important to investigate how obesity-driven inflammation influences Pa immune biology. Understanding these interactions will be critical for optimizing vaccine formulations to ensure robust and durable protection in obese individuals, thereby addressing a significant gap in current vaccine research.

Because of the public health risk posed by Pa, we developed a protein subunit vaccine against Pa incorporating 2 highly conserved proteins of the type III secretion system (T3SS), PcrV and PopB, which are the tip and the first of 2 translocator proteins of the Pa T3SS, respectively. The fusion of PcrV and PopB, forming Pa fusion (PaF), elicits a robust immune response, which is further enhanced by fusion of the LTA1 subunit of labile toxin (LT) from enterotoxigenic *Escherichia coli*, leading to the development of self-adjuvanting L-PaF.[22,23] Additionally, L-PaF has been formulated as a squalene-based oil-in-water (o/w) nanoemulsion with or without the nontoxic Toll-like receptor 4 (TLR4) agonist BECC438b, a biologically derived lipid A analogue.[23–26] Evaluation of this formulation in multiple inbred and outbred murine models confirmed the vaccine's efficacy and identified immune correlates of protection, including the presence of opsonophagocytic immunoglobulins and IL-17A.[22,23,25] Furthermore, our findings indicate that the anti-Pa immune response is influenced by the lung microenvironment, with enhanced protection as the lung locally regulates immune homeostasis.[25–27] This effect was examined across both young and elderly murine populations, demonstrating age-related differences in vaccine-induced immunity.[26]

In this study, we evaluate the protective efficacy of the L-PaF vaccine formulation in a diet-induced obese (DIO) mouse model and investigate the key immune cell populations involved in mediating the immune response. We systematically compare the immune responses among high-fat diet (HFD; 60% fat), a metabolically matched low-fat diet (LFD; 10% fat), and regular laboratory chow (RC; 3% to 4% fat) fed mice to determine how metabolic status influences vaccine efficacy. While L-PaF immunization elicited robust humoral and cellular responses across all groups, HFD mice demonstrated markedly impaired antibody function, characterized by notably low IgA titers, significantly compromised germinal center (GC) formation, and a marked reduction in lung-resident memory B (Brm) cells. In contrast, however, we identify an increased population of lung tissue-resident memory T (Trm) cells in immunized HFD mice, which appears to contribute to protection against Pa colonization, particularly in the absence of effective humoral immunity.

Materials and methods

Squalene was obtained from Echelon Biosciences (Salt Lake City, UT, USA), and BECC438b (hereafter referred to as BECC) was prepared following previously established protocols.[25] All buffers and chemicals utilized in this study were of reagent-grade quality.

Protein purification and vaccine formulation

L-PaF was purified using standard immobilized metal affinity chromatography and Q anion exchange chromatography, followed by dialysis with 0.05% Lauryldimethylamine oxide and storage at −80 °C. All proteins were produced in accordance with the standard operating procedures established in our laboratory.[22,23,28,29] The o/w emulsion formulations, referred to as MedImmune Emulsion (ME), were prepared by homogenizing squalene (8% by weight) and polysorbate 80 (2% by weight) to achieve a uniform oil phase. Histidine (40 mM, pH 6) and 20% sucrose were then incorporated into the oil phase, resulting in a milky emulsion designated as 4× ME. BECC438b (0.5 mg/mL) was solubilized in 0.5% triethylamine (pH 7.2) before incorporation. L-PaF was added to the final formulation, designated L-PaF/ME/BECC, which includes BECC438b as an adjuvant.[30]

Animals

C57BL/6J (strain 000664), C57BL/6J DIO (strain 380050), and C57BL/6J DIO control (strain 380056) male mice of at least 16 weeks of age were purchased from The Jackson Laboratory.[31] After delivery, mice were given a week to acclimate, and then they were maintained on their respective diets: RC (Lab Diets, cat # 5053; ∼4.5% fat) for C57BL/6J, HFD chow (Research Diets, cat # D12492; 60% fat) for C57BL/6J DIO, and an HFD-matched LFD chow (Research Diets, cat #D12450K; 10% fat) for C57BL/6J DIO control. The background nutrients in the RC diet were not matched to the 2 fat-containing diets but were included in some of these experiments because this is the diet fed to mice used in previous studies done in our laboratory.

Immunization

Mice were immunized intranasally with 30 µL containing PBS, 1 µg of L-PaF in ME (L-PaF 1/ME), 5 µg of L-PaF in ME (L-PaF 5/ME), 1 µg of L-PaF with 0.5 µg BECC in ME (L-PaF 1/BECC 0.5/ME), 5 µg of L-PaF with 0.5 µg BECC in ME (L-PaF 5/BECC 0.5/ME), 1 µg of L-PaF with 1 µg BECC in ME (L-PaF 1/BECC 1/ME), and 5 µg of L-PaF with 1 µg BECC in ME (L-PaF 5/BECC 1/ME).

Formulations were administered on day 0 as a prime dose, followed by booster doses on days 14 and 28. Mice were bled on 0, 28, 42, and 56 days postimmunization to prepare serum.

Ethics statement

All animal studies were carried out in accordance with the University of Missouri–Columbia Institutional Animal Care and Use Committee animal use statement (protocol number 38241).

ELISA

Serum IgG and IgA responses were determined against the vaccine components PcrV and PopB using 96-well plates coated with 1 μg/mL of PcrV or PopB. Protein binding was allowed for 3 hours, followed by blocking with 10% nonfat dry milk overnight at 4 °C. Mouse serum was added and incubated for 1 hour at 37 °C, followed by washing with PBS-Tween 20. Goat anti-mouse IgG (1:1,000)/IgA (1:4,000) (cat # OB1040-05 for IgA from Southern Biotech; cat # 5450-0011 [474-1806] for IgG from Sera Care) secondary antibodies conjugated with horseradish peroxidase (HRP) were added followed by the addition of TMB substrate (3,3′,5,5′-tetramethylenebenzidine). Phosphoric acid was used to stop the reaction and ELISA units per mL (EU/mL) were used to compute endpoint titers. Similarly, IgG1 and IgG3 subclasses were determined using the goat anti-mouse IgG1 (1:1,000) and rat anti-mouse IgG3 (1:4,000) (Southern Biotech, cat # 1070-05 and 1191-05, respectively) tagged with an HRP-conjugated secondary antibody.

Opsonophagocytic killing assay

The opsonophagocytic killing (OPK) assay was performed as described previously.[25] In brief, 90% confluent J774.1 mouse macrophage cells were used for the serum opsonization assay. Then, 2×10^7 mPa-0831 was prepared in 10% bovine serum albumin (Sigma, St. Louis, MO, USA) containing minimal essential medium (Thermo Fisher, Waltham, MA, USA) and added to the macrophages at a multiplicity of infection of 0.1. Sera obtained from each mouse group at 42 days postimmunization were subjected to heat inactivation at 56 °C for 30 minutes. The samples were subsequently diluted 1:500 and mixed with bacteria and macrophages in equal proportions (1:1:1), yielding a final volume of 300 μL. Following incubation at 37 °C for 30 minutes, serial dilutions were performed for all technical quadruples and plated onto *Pseudomonas* isolation agar. After overnight incubation, the following formula was used to calculate percentage of bacterial killing:

$$\frac{\{(CFU\ at\ T0) - (CFU\ at\ T30)\}}{(CFU\ at\ T0)} \times 100$$

Pseudomonas aeruginosa infection

The Pa cultures were prepared as previously described.[25] In brief, an overnight culture of mPa-0831 was inoculated into fresh low salt Luria Broth at a dilution of 1:100 until the absorbance (A600) reached 0.34 to 0.35. Intranasal administration of 4×10^7 CFU/30 μL, 1×10^8 CFU/30 μL, and 4×10^8 CFU/30 μL mPa-0831 were used to infect RC, LFD, and HFD mice, respectively. Lungs were harvested approximately 16 to 18 hours postinfection. The bacterial challenge dose depended upon the predetermined lethal dose 50%, which was influenced by the body weight and immune status of the animals. Experiments were performed to determine the appropriate challenge dose that allowed us to observe vaccine-mediated protection.

Organ processing

In prechallenge experiments, mouse lungs were aseptically collected on day 56 after the first immunization. In postchallenge experiments, mouse lungs were collected 16 hours after pulmonary challenge. Lungs were dissociated using the MACS Lung Dissociation kit (Miltenyi Biotec, Gaithersburg, MD, USA). The red blood cells (RBCs) were lysed using the RBC lysis solution provided in the kit, and lung cell suspensions were prepared by filtering through a 70-μm filter. Cells were adjusted to the desired concentration for further use in MSD cytokine analysis (Meso Scale Discovery, Rockville, MD, USA) and bacterial enumeration. For flow cytometry studies and some of the prechallenge studies, spleens were collected from mice, processed using MACS Spleen Dissociation kit (Miltenyi Biotec) into single-cell suspensions, and diluted to the desired concentrations.

Cytokine analysis

Single-cell suspensions of lung cells or splenocytes were incubated at 37 °C for 48 hours with or without PcrV or PopB at a concentration of 10 μg/mL. Supernatants were collected and analyzed using U-PLEX assay kits to quantify cytokine concentrations. Prechallenge lung samples were assessed for IFN-γ, IL-17A, IL-2, IL-22, IL-6, TNF-α, and IL-12p70 concentrations. In contrast, postchallenge unstimulated lung samples were evaluated for TNF-α, IL-6, IL-1β, and IL-15. Cytokine concentrations were determined according to the manufacturer's instructions (Meso Scale Discovery).

FTY720 treatment

Mice received intraperitoneal injections of FTY720 (Tocris Bioscience, cat # 6176) (1 mg/kg) or PBS as indicated beginning 3 days prior to infection.

Flow cytometric analysis

For splenocytes, GC B cells, T follicular helper (TFH) cells, and T follicular regulatory (TFR) cells were also assessed. All samples were subjected to live-dead staining using Fixable Viability Stain 620 (BD Biosciences, cat # 564996) for 15 minutes at room temperature. The cells were washed and stained for surface markers on ice for 20 minutes. After surface staining, cells were washed with stain buffer (prepared in the laboratory; 1% FBS and 0.09% sodium azide in HBSS) twice, and then they were either subjected to acquisition or were further processed for intracellular staining. For intracellular staining, cells were fixed and permeabilized with 1× Fix/Perm buffer followed by washing with 1× Perm/Wash buffer of Transcription Factor Buffer Set (BD Pharmingen, cat #

562574). Cells were then stained with the intracellular antibody mix and incubated on ice for 20 minutes. Samples were washed and data acquired on a Bigfoot Cell Sorter (Thermo Scientific) at the University of Missouri Laboratory for Infectious Disease Research Immunology Core. Manual gating of flow cytometry data was done using FlowJo v10.10.0.

The markers used in cell characterization were as follows (all antibodies are from BD Biosciences, unless otherwise stated):

- Macrophages: CD40 (cat # 561846), CD11c (cat # 568971), F4/80 (cat # 569223), CD64 (cat # 558539).
- Classical dendritic cells type 2 (cDC2): CD86 (cat # 553691), CD40 (cat # 561846), CD11c (cat # 568971), MHC-II (I-A/I-E, cat # 743870), CD3 (cat # 563565), CD19 (cat # 563557), CD64 (cat # 558539), F4/80 (cat # 569223), CD24 (cat # 757887).
- AMs: CD11c (cat # 746392), MHC-II (I-A/I-E, cat # 746086), and Siglec-F (cat # 552126).
- GC B cells: CD138 (cat # 563147), B220 (cat # 756542), CD19 (cat # 562701), GL7 (cat # 570602), Bcl6 (cat # 563581), IRF4 (cat # 566649).
- TFH and TFR cells: CD4 (cat # 558107), B220 (cat # 746206), CXCR5 (cat #5 61988), PD1 (cat # 568608), Bcl6 (cat # 563581), Foxp3 (cat # 567458).
- Trm cells: CD3 (cat # 555274), CD4 (cat # 558107), CD44 (cat # 568507), CD62L (cat # 570282), CD69 (cat # 569688), CD103 (cat # 758108).
- Brm cells: CD19 (cat # 562701), B220 (cat # 756542), CD38 (cat # 755623), IgD (cat # 405708, BioLegend), CD69 (cat # 569688), CXCR3 (cat # 753433), CD80 (cat # 746775), PDL2 (cat # 752609).

Data and statistical analyses

GraphPad Prism v10.1 software was used to process data and to perform statistical tests. FlowJo v10.1.1 software was used to analyze flow cytometry data. Normality was checked using the Shapiro–Wilk test. Data followed a nonparametric distribution. Comparisons between 2 groups were assessed by the Mann–Whitney U test. Three or more groups were compared by either Kruskal–Wallis test with Dunn multiple comparison post hoc test or 2-way ANOVA following the uncorrected Fisher least significant difference/Tukey multiple comparison test. PBS was used as control in all cases. Studies were conducted with 5 mice per group unless otherwise stated in the text or figure legends ($^{*}P < 0.05$, $^{**}P < 0.01$, $^{***}P < 0.001$, $^{****}P < 0.0001$).

Results

L-PaF/ME/BECC is immunogenic in diet-induced obese mice

Humoral response

Previous studies from our group showed that L-PaF, used alone or with ME and BECC, provides strong protection against Pa in diverse mouse strains.[23,25] To assess the immunogenicity of L-PaF/ME with or without BECC in an obese mouse model, we immunized all the 3 cohorts of mice (HFD, LFD, and RC) with varying concentrations of L-PaF formulated with ME and with or without BECC using a prime-boost-boost regimen, with 14 days between each dose. We collected serum samples for this dose escalation experiment as described in the Materials and methods. We observed that total IgG levels in the sera of mice were largely consistent across all diet groups; however, these levels began to wane in the HFD mice relative to the other 2 groups (Fig. 1A–F). The L-PaF 5/ME/BECC 0.5 group showed higher anti-PcrV and anti-PopB IgG titers, closely followed by the L-PaF 5/ME and L-PaF 5/ME/BECC 1 groups. Anti-PopB titers demonstrated greater variability than the anti-PcrV titers. For IgA, initial levels were comparable across cohorts, though the HFD mice exhibited a noticeably more rapid decrease in IgA titers (Fig. 1G–L). Both immunogens elicited class switching to IgA, though to a lesser extent than IgG, and induced similar IgA levels against PcrV and PopB across cohorts. This dose-escalation study underscores the immunogenic potential of L-PaF when formulated in an o/w emulsion nanoparticle (ME) with or without the TLR4 agonist BECC.

Cellular responses

To assess cellular immune responses, we analyzed lung tissues from mice immunized with L-PaF/ME with or without BECC for cytokine production. In HFD and LFD mouse lungs, we found that antigenic stimulation with PcrV or PopB was necessary to elicit detectable levels of IFN-γ and IL-17A (Fig. 2). In contrast, for RC mice, baseline (unstimulated) levels of these cytokines were only elevated after BECC was incorporated into the formulation (Fig. 2A, B, G, H, M, N). We observed similar trends for IL-2 and IL-22 (Fig. 2C, D, I, J, O, P); however, all dietary groups exhibited elevated IL-6 baseline levels (Fig. 2E, K, Q). TNF-α levels were comparable between LFD and RC mice but were notably lower in HFD mice (Fig. 2F, L, R). Thus, L-PaF/ME/BECC effectively activates immune cells to promote cytokine production, noting that dietary variations influence the baseline and antigen-stimulated responses.

Protective efficacy of L-PaF/ME/BECC in vitro and in vivo

We evaluated the protective efficacy of L-PaF formulations in vitro through OPK of Pa by serum immunoglobulins. In HFD mice, we observed significantly enhanced OPK activity in the L-PaF 5/ME/BECC 1 group, while formulations lacking BECC or containing lower concentrations of L-PaF failed to elicit significant OPK activity (Fig. 3A). L-PaF 5/ME/BECC 0.5 and L-PaF 1/ME/BECC 1 exhibited moderate levels of killing compared to controls. In LFD mice, sera from both L-PaF 5/ME/BECC 0.5 and L-PaF 5/ME/BECC 1 had significantly higher OPK activity (Fig. 3B). Similarly, we found that OPK activity was significantly higher in RC mice immunized with L-PaF 5/ME/BECC 0.5, L-PaF 1/ME/BECC 1, and L-PaF 5/ME/BECC 1 (Fig. 3C). These findings suggest that L-PaF 5/ME/BECC 1 is the most effective formulation for HFD and LFD mice, while L-PaF 5/ME/BECC 0.5 appears optimal for RC mice. However, to maintain consistency in subsequent in vivo protection studies, we selected L-PaF 5/ME/BECC 1 as the L-PaF formulation across all cohorts.

Consistent with our previous studies demonstrating a correlation between in vitro OPK activity and in vivo bacterial lung burden,[22,23,25] immunization of all 3 dietary groups with the L-PaF formulation resulted in a significant reduction in lung bacterial

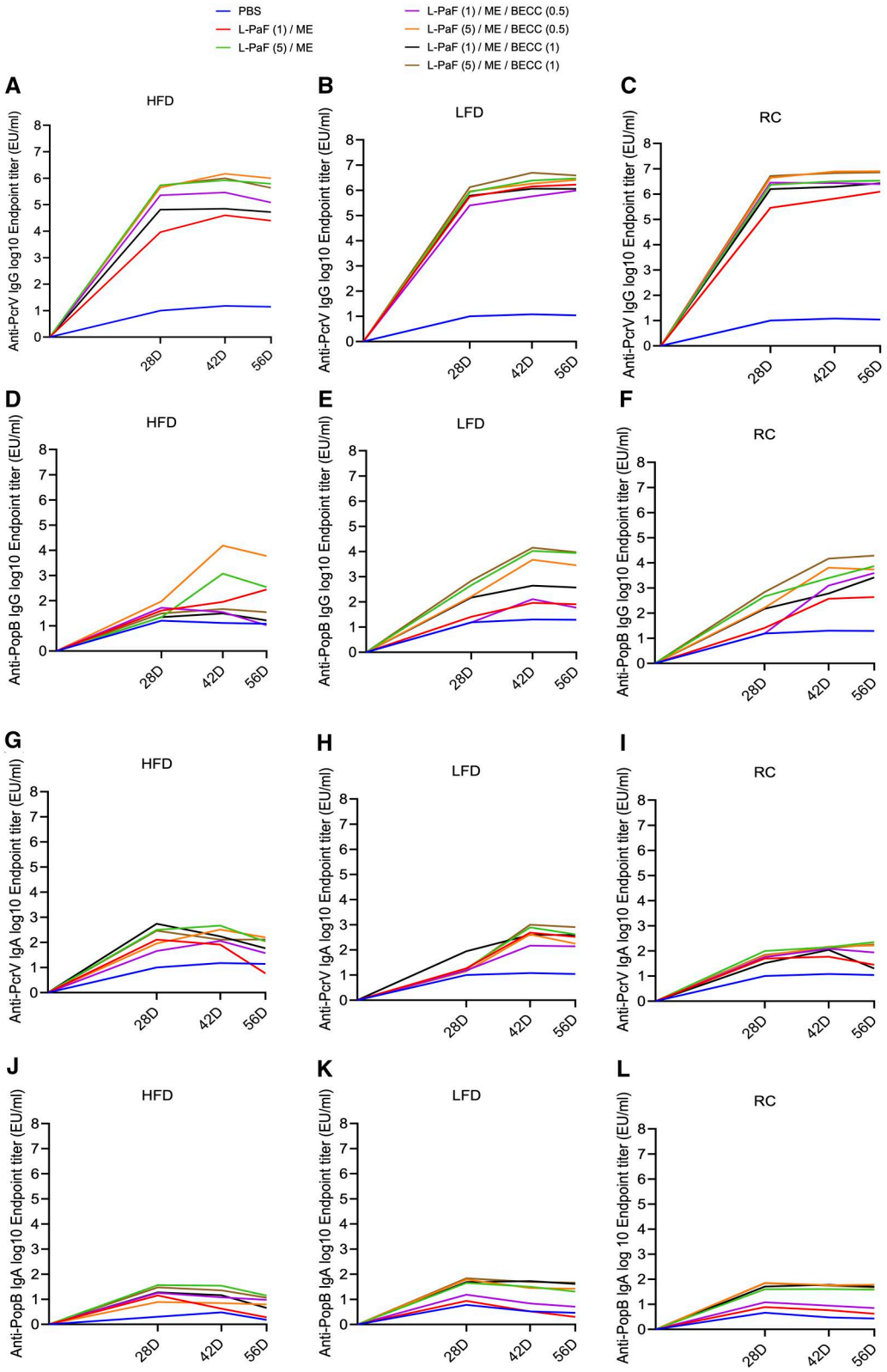

Figure 1 Kinetics of serum IgG and IgA. HFD, LFD, and RC mice were vaccinated on days 0, 14, and 28. Serum samples collected over time were analyzed for anti-PcrV and anti-PopB immunoglobulins over the course of immunization. Anti-PcrV IgG (A–C) and IgA (G–I), along with anti-PopB IgG (D–F) and IgA (J–L), are shown for HFD, LFD, and RC mice. Each data point represents pooled serum from 10 mice per group ($n = 10$), and titers are expressed as EU/mL. Statistical analyses were performed using a 2-way ANOVA (Dunnett test) with all the *P* values presented in Table S1.

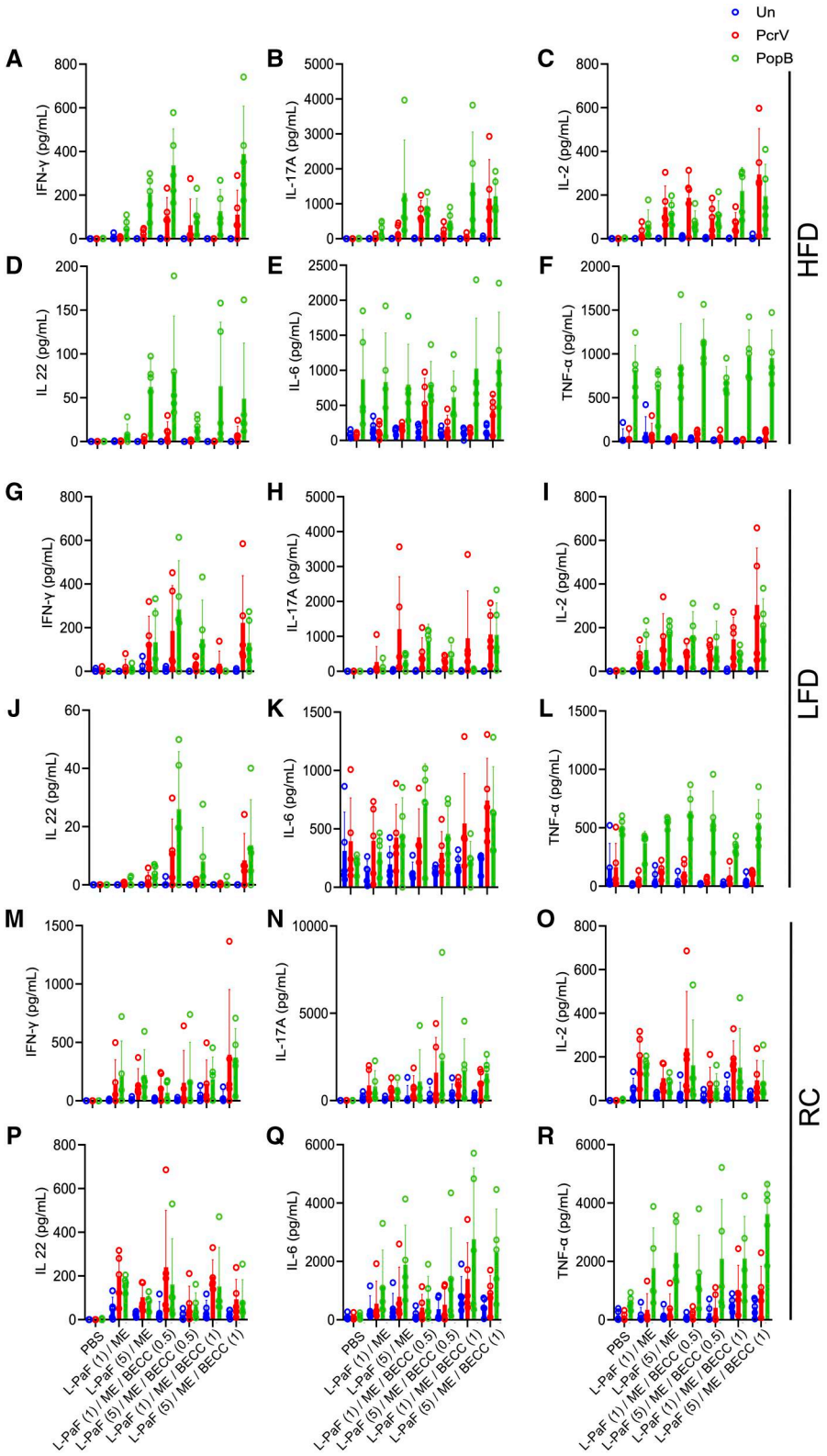

Figure 2 Lung-derived cytokine responses following immunization with L-PaF/ME with or without BECC across different dietary groups. Lung single-cell suspensions from immunized mice of HFD (A–F), LFD (G–L), and RC (M–R) were either stimulated ex vivo with PcrV or PopB, or left unstimulated (Un), and supernatants were analyzed for IFN-γ, IL-17A, IL-2, IL-22, IL-6, and TNF-α after 48 hours. Each dot represents actual values and error bars show SD ($n = 5$/group). Statistical comparisons were performed using 2-way ANOVA following Tukey test. All P values are presented in Table S2 rather than in this figure for visual clarity (*$P < 0.05$, **$P < 0.01$).

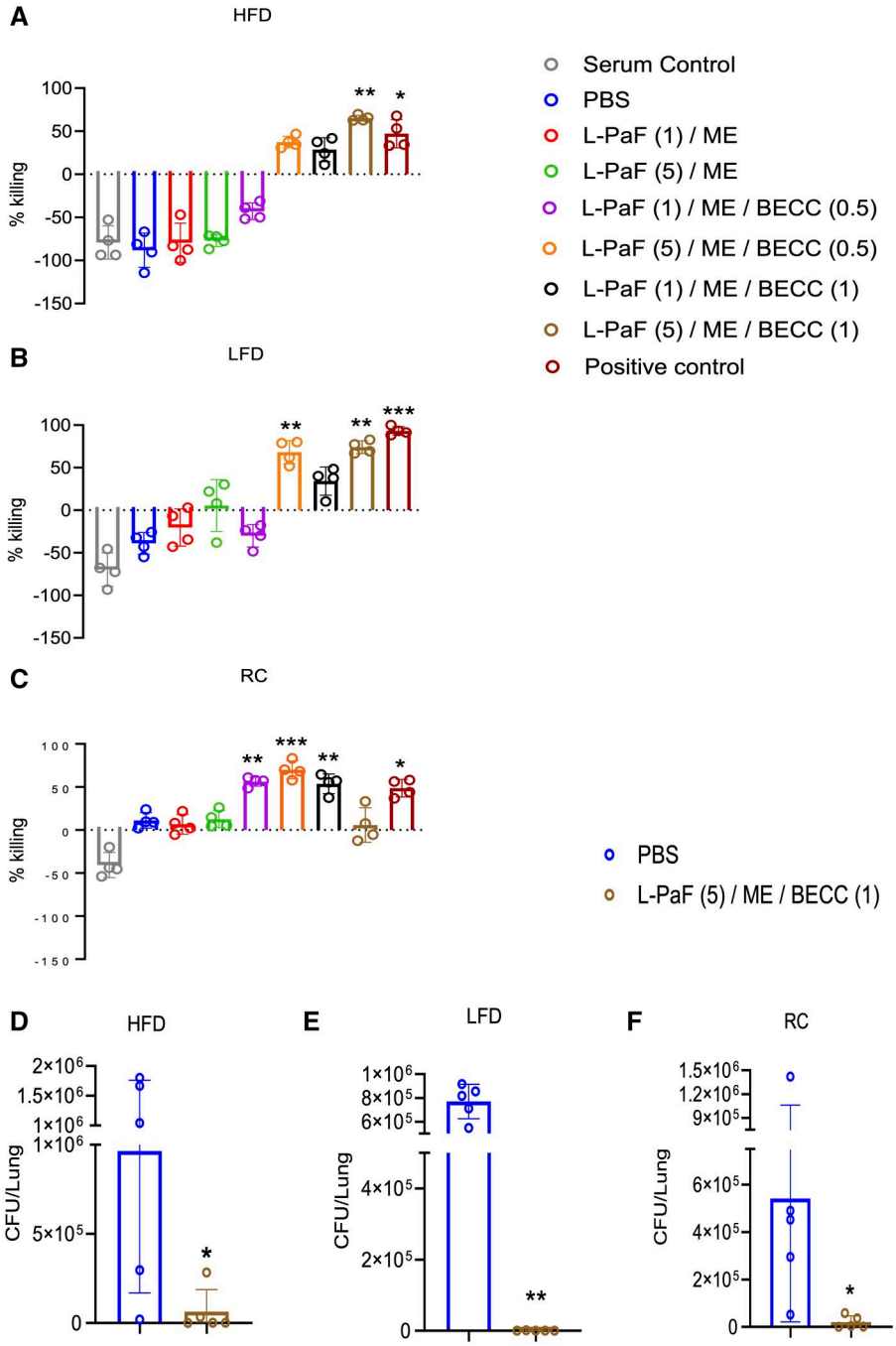

Figure 3. In vitro and in vivo protection conferred by L-PaF/ME/BECC immunization across dietary groups based on opsonophagocytic killing (OPK). OPK of strain mPa08-31 by J774.1 macrophages was evaluated using heat-inactivated serum collected on day 42 postimmunization from HFD (A), LFD (B), and RC (C) mice immunized with the different L-PaF/ME/BECC formulations. Data points represent technical replicates from pooled serum samples, with error bars indicating SD. Statistical analysis was performed using Kruskal–Wallis test followed by Dunn multiple comparisons. In vivo protective efficacy was assessed by quantifying bacterial burden (CFU/lung) in HFD, LFD, and RC mice (D–F) 16–18 hours postchallenge. Each data point represents an individual mouse ($n = 5$), and error bars represent SD. Statistical significance between PBS and immunized groups was determined using the Mann–Whitney U test (*$P < 0.05$, **$P < 0.01$, ***$P < 0.001$).

burden compared to PBS-immunized mice (Fig. 3D–F). Additionally, immunization with the L-PaF formulation significantly upregulated antigen-specific IgG titers, including IgG1 and IgG3 subtypes, against both PcrV and PopB relative to PBS immunization. While a significant increase in antigen-specific IgA was detected in the L-PaF formulation–immunized groups compared to PBS immunized, IgA titers in the HFD group were notably lower than those in LFD and RC mice (Fig. S1A–C).

To further understand the postchallenge immune environment and the nature of the inflammatory response, we analyzed lung cell supernatants for TNF-α, IL-6, IL-1β, and IL-15. This analysis revealed a pronounced proinflammatory cytokine

response for HFD (Fig. S2A–D) and RC (Fig. S2I–L) mice immunized with the L-PaF formulation. Conversely, in LFD mice (Fig. S2E–H), immunization with the L-PaF formulation resulted in significantly attenuated levels of TNF-α and IL-1β compared to PBS controls. Collectively, these findings suggest that higher concentrations of both L-PaF and BECC are necessary to achieve optimal protection in HFD and LFD mice compared to RC mice.

Heterogeneous activation and functional competence of lung antigen-presenting cells in response to immunization with L-PaF formulation

A single-cell study from our laboratory has demonstrated that antigen-presenting cells (APCs), that is, cDC2s and macrophages, are activated via the upregulation of CD86 and CD40 (manuscript under review). Given that these APCs serve as the primary sentinels for antigen uptake and the initiation of host immune responses against pathogens, we quantified their frequencies and activation status within the lung. To determine if vaccination could overcome obesity-associated innate immune defects, we characterized the activation state of lung APCs in HFD and LFD mice. RC mice were used solely to establish a baseline for comparison with previous studies and were not included in further comparative analyses. In both HFD and LFD mice, we observed a significant increase in the frequency of activated $CD40^+CD86^+$ cDC2s in the lungs of L-PaF formulation–immunized mice compared to PBS-immunized mice (Fig. 4A, B). Similarly, analysis of macrophage populations revealed a higher frequency of activated macrophages in L-PaF formulation–immunized mice relative to PBS-immunized mice, albeit not statistically significant (Fig. 4C, D), again with the magnitude being greater in LFD mice. These findings suggest that the L-PaF formulation effectively stimulates APCs, which are critical for initiating host defense mechanisms against Pa, to differing degrees in both populations.

Because IL-12p70 is a key cytokine secreted by activated APCs,[32,33] we next chose to assess lung APC functionality by examining the IL-12p70 relationship with activated cDC2s and macrophages. We found the upregulation of APCs to correlate with IL-12p70 levels from PcrV-stimulated lung (Fig. S3A). This suggests that the vaccine promotes a functional APC phenotype associated with the production of Th1-polarizing cytokines, consistent with the established role of activated APCs in driving type 1 cellular immunity.[34,35] Meanwhile, macrophage activation strongly correlated with IL-12p70 levels in LFD mice immunized with L-PaF formulation; however, no such correlation was observed in the HFD mice.

To specifically address macrophage contributions, we characterized AMs, a category of lung macrophages known for their role in antigen presentation and for orchestrating local immune responses through MHC class II (MHCII) expression.[36,37] We isolated lung AMs 56 days post–initial immunization and analyzed them for MHCII expression. We observed no significant differences between the PBS and L-PaF vaccinated groups for $MHCII^+$ AMs in HFD (Fig. 4E). In LFD mice immunized with the L-PaF formulation, the expression of MHCII on AMs was elevated compared to PBS controls, meeting a 90% confidence threshold ($P = 0.0952$) although not reaching the standard 95% significance level (Fig. 4F). Interestingly, the overall abundance of $MHCII^+$ AMs was higher in the HFD cohort compared to their LFD counterparts. Collectively, these data suggest that an HFD may differentially impact the activation and antigen-presenting capacity of lung macrophages, potentially influencing the overall cytokine environment and downstream immune responses.

Impaired GC formation is due to aberrant TFH/TFR cells in obese mice

To understand the inconsistent IgA titers in HFD mice, we focused on GC formation and characterized the GC B cells and TFH cells, key drivers of humoral immunity. We collected spleens from the immunized HFD and LFD cohorts 9 days after the final immunization. Regardless of immunization with the L-PaF formulation or PBS, the frequency of GC B cells was significantly lower in HFD mice compared to LFD mice (Fig. 5A). Furthermore, immunization with L-PaF formulation failed to induce an increase in GC B-cell frequency in HFD mice, whereas robust upregulation was evident in LFD mice. Similarly, plasma cell (PC) responses were impaired in HFD mice with no significant difference being observed between L-PaF formulation– and PBS-immunized groups (Fig. 5B). In contrast, LFD mice showed a substantial overall increase in PCs following immunization with L-PaF formulation with a $P = 0.07$. With respect to TFH cells, we observed no increase in the frequency of TFH cells following immunization with L-PaF formulation in HFD mice, whereas a significant upregulation was observed in LFD mice (Fig. 5C). These findings suggest that the lower antibody responses in HFD mice may be attributed to defective GC B, PC, and TFH cell development.

Because TFR cells are key players in shaping GCs, we analyzed their frequency and found a decrease in TFR cells in HFD mice compared to LFD mice immunized with the L-PaF formulation (Fig. 5D). This may indicate a dysregulated GC microenvironment during obesity. Furthermore, we analyzed the expression of both PD-1 and CXCR5 on TFH as well as TFR cells, because these markers are crucial for their localization within the GC and for regulating interactions with GC B cells.[38] Notably, we observed lower CXCR5-expressing $CD4^+Bcl6^+$ and $CD4^+Bcl6^+Foxp3^+$ cells in HFD mice compared to LFD mice immunized with the L-PaF formulation (Fig. S4C). Conversely, PD-1 expression remained consistently high on $CD4^+Bcl6^+$ and $CD4^+Bcl6^+Foxp3^+$ cells in HFD mice, but we observed it was significantly downregulated in LFD mice after immunization with the L-PaF formulation (Fig. 5E, F). Therefore, persistent PD-1 expression may interfere with CXCR5 upregulation, thereby impairing B-cell–T-cell interactions within GCs and contributing to the suboptimal humoral response observed in obese mice.

Differential Trm induction in the lung following L-PaF formulation immunization in LFD and HFD mice

To assess whether immunization with the L-PaF formulation promotes the establishment of resident memory cells in pulmonary tissue, we harvested lungs from HFD and LFD mice 56 days post–first immunization. Analysis of lung-resident Brm cells revealed no statistically significant difference in Brm numbers between the vaccinated and PBS-treated groups in either HFD (Fig. 6A) or LFD mice (Fig. 6B). Given the established role of Brm cells in mediating rapid in situ antibody production, we assessed IgG levels in lung supernatants. While LFD mice exhibited a significant increase in IgG titers, no such increase was observed in

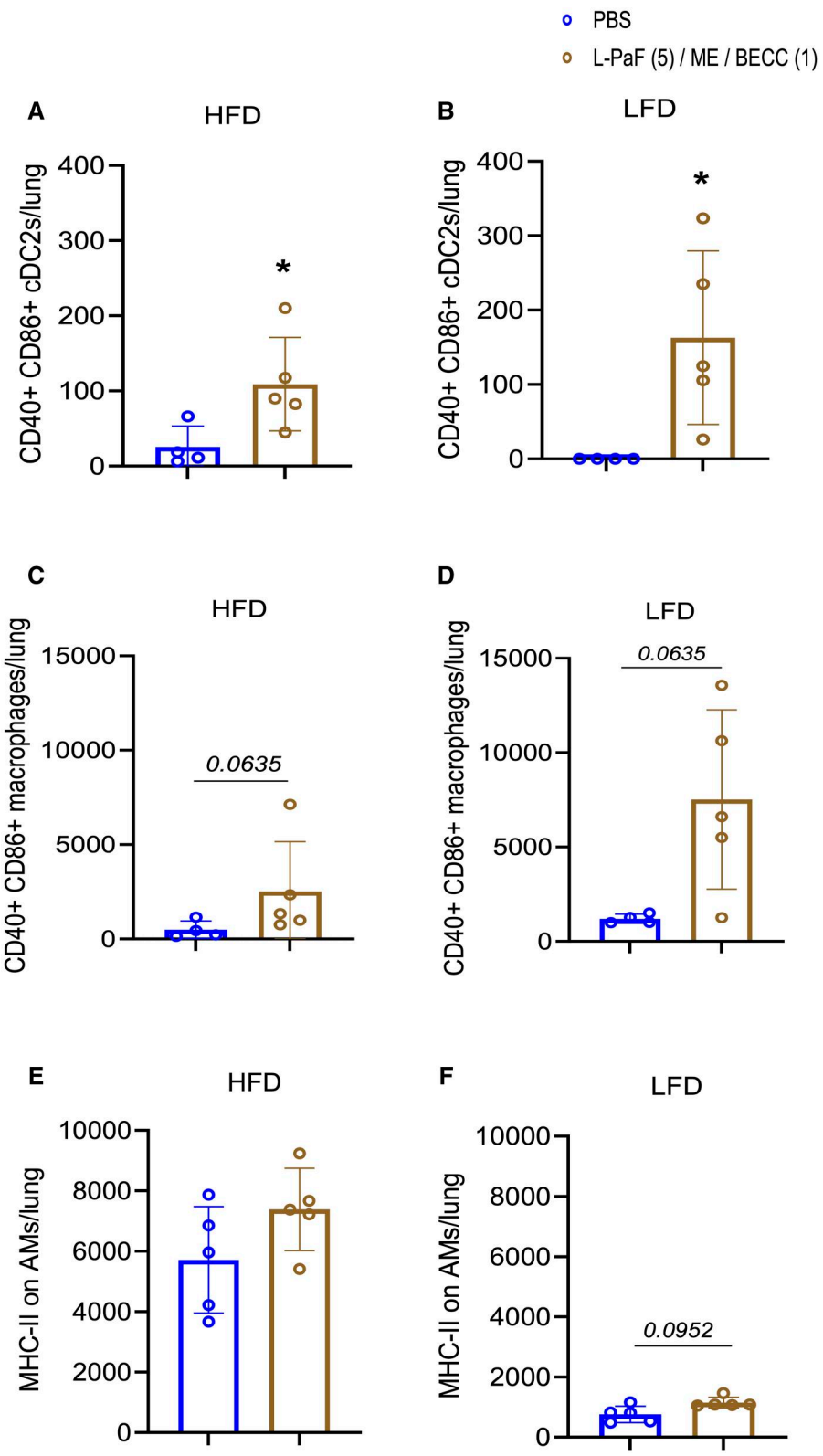

Figure 4. Activation and characterization of lung antigen-presenting cells following L-PaF/ME/BECC immunization in HFD and LFD mice. Flow cytometry was performed on lung single-cell suspensions collected 2 days post–final immunization to assess the frequency and activation of cDC2s (A, B) and activated macrophages (C, D) in both HFD and LFD mice compared to controls. Alveolar macrophages (AMs) were analyzed for MHCII expression 56 days post–initial immunization in HFD (E) and LFD (F) mice. Each data point represents an individual mouse ($n = 5$), and error bars represent SD. Statistical significance between PBS and immunized groups was determined using the Mann–Whitney U test (*$P < 0.05$). All dot plots are presented in Fig. S5.

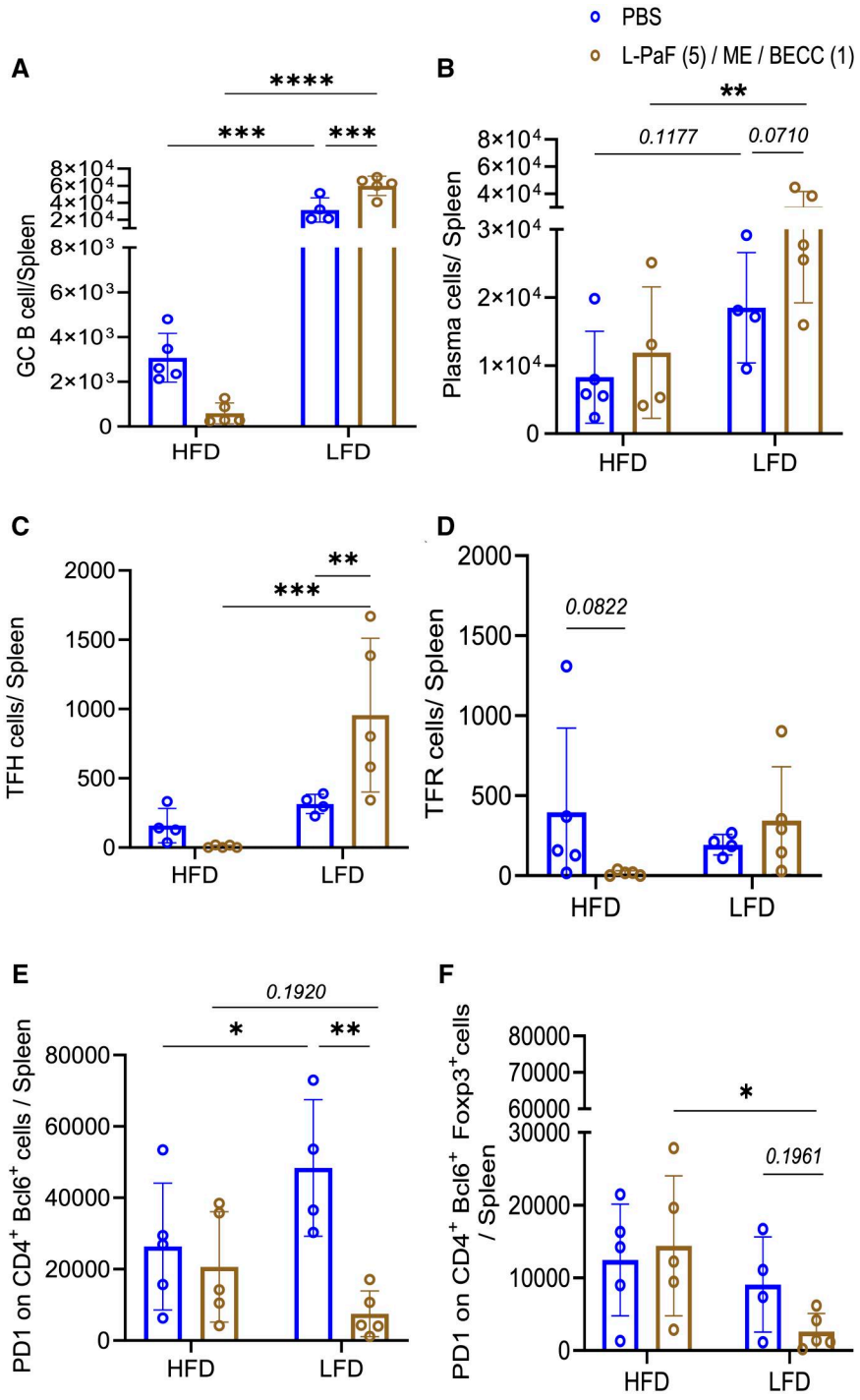

Figure 5. Obesity impairs vaccine-induced germinal center (GC) and T-cell response. Flow cytometric analysis was performed on spleen single-cell suspensions collected 9 days post–final immunization. Frequency of GC B cells (A), plasma cells (B), TFH cells (C), and TFR cells (D) in the spleen LFD and HFD mice. PD-1 expressing $CD4^+Bcl6^+$ (E) and $CD4^+Bcl6^+Foxp3^+$ (F) across the experimental groups. Each data point represents an individual mouse ($n = 4$ or 5). Error bars represent SD. Statistical comparisons were performed using 2-way ANOVA following uncorrected Fisher least significant difference test (*$P < 0.05$, **$P < 0.01$, ***$P < 0.001$, ****$P < 0.0001$). All of the dot plots are presented in Fig. S4.

HFD mice (Fig. S5A, top panel, left). To investigate this discrepancy, expression of PDL2 and CD80 on Brm cells was examined because these markers are associated with the rapid differentiation of antibody-secreting cells upon antigen reexposure.[39] Consistent with the elevated IgG levels, LFD mice showed a significant upregulation of $PDL2^+CD80^+$ Brm cells, a response that was absent in HFD mice (Fig. S5A, top panel, middle and right). Despite the observed disparities in Brm responses, a significant increase in lung-resident Trm cells was detected in both HFD and LFD mice (Fig. 6C, D).

The pivotal role of IL-2 in Trm formation and maintenance has been demonstrated by others.[40,41] To assess IL-2 production

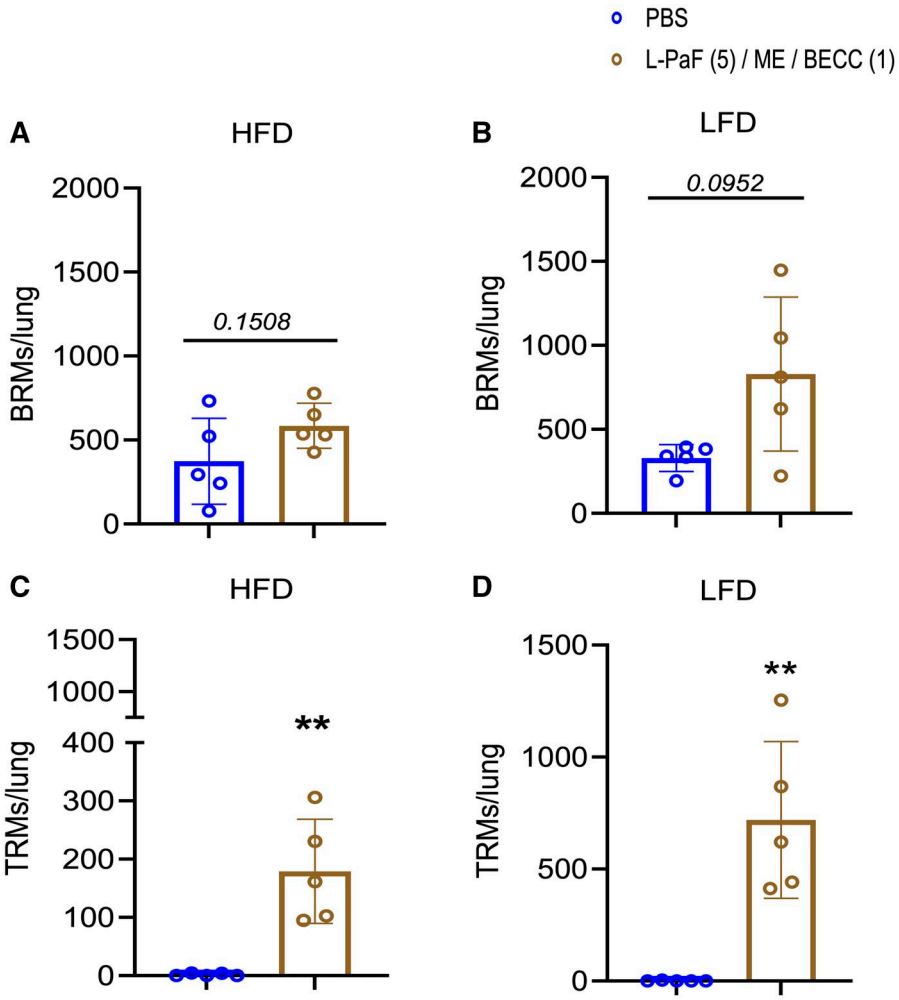

Figure 6. Induction of lung-resident memory T cells (Trms) and B cells (Brms) following L-PaF/ME/BECC immunization in HFD and LFD mice. Lung tissues were harvested 56 days post–initial immunization to assess the presence of tissue-resident memory cells using flow cytometry. Brm and Trm populations in both HFD (A, C) and LFD (B, D) mice prior to infection. Each data point (A–D) represents an individual mouse ($n = 5$) and error bars represent SD. Statistical significance between PBS and immunized groups was determined using the Mann–Whitney U test (**$P < 0.01$). All the flow cytometry dot plots are presented in Fig. S5B and C.

here, lung cells were stimulated with either PcrV or PopB. Both antigens significantly upregulated IL-2 production in lung cells derived from HFD and LFD mice immunized with L-PaF formulation (Fig. S5A, second row of panels). Nevertheless, correlation analyses revealed that PcrV-stimulated IL-2 production was positively correlated with lung Trm cells in both HFD and LFD mice, while only PopB-stimulated IL-2 production correlated positively with lung Trm cells in LFD mice and not in HFD mice (Fig. S5A, third row of panels).

Early secondary protection against Pa is maintained in the absence of circulating T-cell recruitment following L-PaF/ME/BECC immunization

To assess whether it is lung Trm cells or circulating T cells that play a predominant role in preventing Pa colonization, we used FTY720 to block T-cell egress from secondary lymphoid organs,[42,43] thereby isolating the role of lung-resident T-cell populations. Analysis of pulmonary $CD3^+CD4^+$ T-cell populations was performed to evaluate the efficacy of FTY720 in restricting the migration of circulating T cells (Fig. S6A). In the absence of FTY720, no significant differences were observed between PBS- and L-PaF formulation–immunized groups in HFD mice (Fig. 7A), whereas L-PaF formulation–immunized LFD mice exhibited a significant increase in pulmonary $CD3^+CD4^+$ T-cell infiltration compared to PBS immunized (Fig. 7B). Upon FTY720 treatment, L-PaF formulation–immunized mice from both diet groups maintained significantly higher $CD3^+CD4^+$ T-cell numbers in the lung relative to their PBS-immunized control. Additionally, FTY720 markedly reduced $CD3^+CD4^+$ T-cell counts in the PBS-immunized group, confirming its role in limiting circulating T-cell migration. These findings suggest that immunization with the L-PaF formulation promotes the accumulation of lung-resident $CD3^+CD4^+$ T cells independent of circulating T-cell input.

To distinguish between naïve and effector/memory subsets, we analyzed CD44 and CD62L[44] expression of the pulmonary $CD3^+CD4^+$ T cells (Fig. S6B). In the absence of FTY720, we observed a higher frequency of $CD44^{low}CD62L^{high}$ circulating naïve

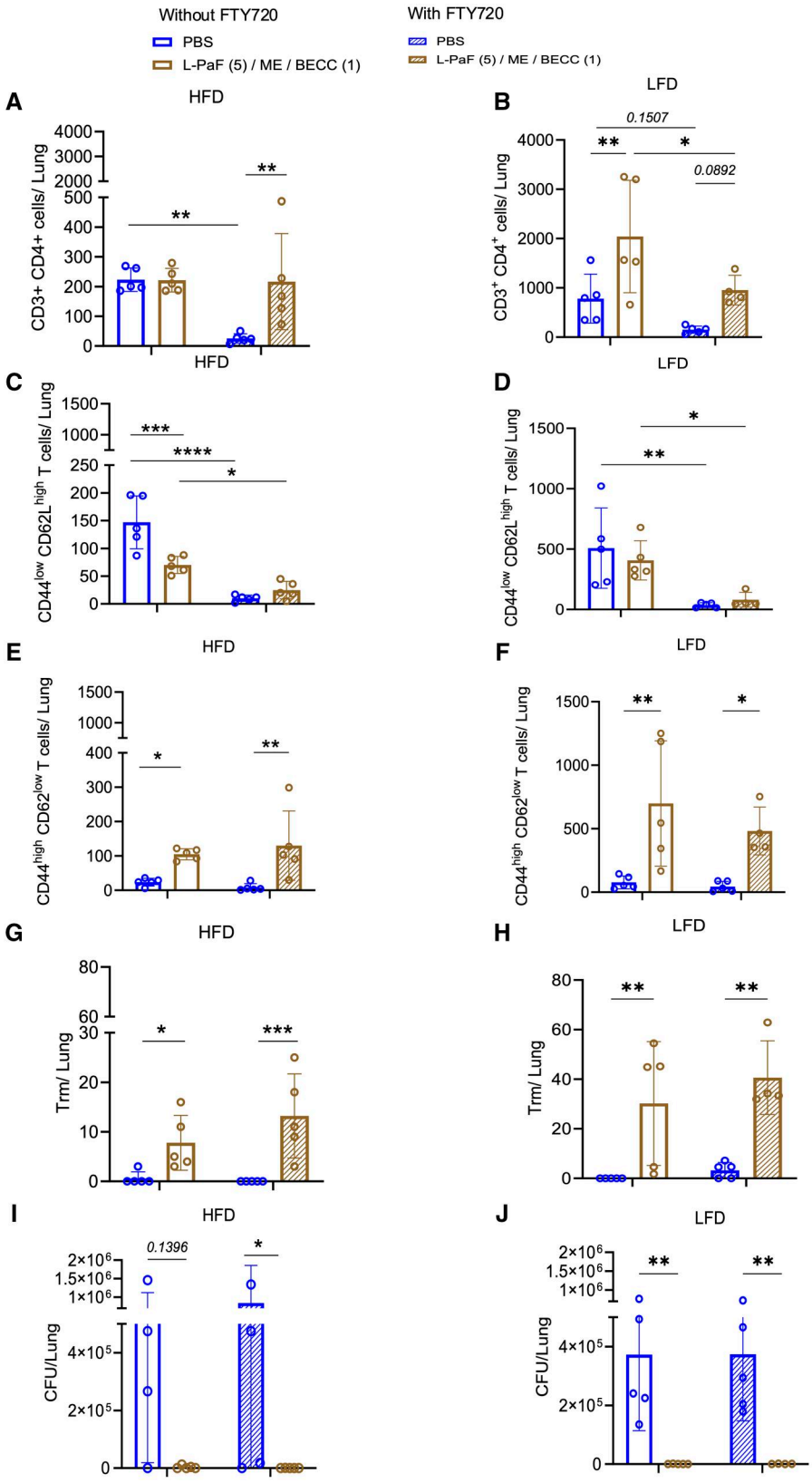

Figure 7. FTY720 treatment distinguishes circulating from lung-resident CD4$^+$ T-cell populations following L-PaF/ME/BECC immunization. Lung tissues were harvested 56 days post–initial immunization following *Pseudomonas aeruginosa* (Pa) infection to assess the presence of tissue-resident memory cells through flow cytometric analysis without or with FTY720 treatment. (A, B) CD3$^+$CD4$^+$ T cells in HFD and LFD mice without or with FTY720 treatment. (C, D) Frequency of CD44^{low}CD62L^{high} naïve CD4$^+$ T cells in the lungs of PBS- and L-PaF/ME/BECC-immunized mice, without or with FTY720. (E, F) Frequency of CD44^{high}CD62L^{low} effector/memory CD4$^+$ T cells in immunized vs control groups under FTY720 treatment. (G, H) Frequency of

(Continued)

Figure 7. Continued
$CD69^+CD103^+$ tissue-resident memory (Trm) $CD4^+$ T cells within the $CD44^{high}CD62L^{low}$ subset in immunized and PBS-treated mice across both diet cohorts. (I, J) Lung burdens following Pa challenge in immunized and control mice without or with FTY720 treatment. Each data point represents an individual mouse ($n = 4$ or 5). Error bars represent SD. Statistical comparisons were performed using 2-way ANOVA following uncorrected Fisher least significant difference test (*$P < 0.05$, **$P < 0.01$, ***$P < 0.001$, ****$P < 0.0001$). All of the dot plots are in Fig. S6B and C.

T cells in PBS-immunized animals compared to those immunized with the L-PaF formulation, while no significant differences were seen in LFD mice (Fig. 7C, D). FTY720 effectively blocked the recruitment of circulating naïve T cells to the lung in both dietary groups. Conversely, L-PaF formulation–immunized mice from both cohorts exhibited a significantly higher frequency of $CD44^{high}CD62L^{low}$ effector/memory T cells compared to PBS-immunized mice, regardless of FTY720 treatment (Fig. 7E, F), suggesting that immunization with L-PaF formulation supports the development of lung-resident memory populations. To evaluate the tissue residency and persistence of pulmonary memory T cells, we then assessed the expression of CD69 and CD103 within the $CD44^{high}CD62L^{low}$ effector/memory population. Mice immunized with the L-PaF formulation, regardless of diet or FTY720 treatment, showed significantly elevated frequencies of $CD44^+CD62L^-CD69^+CD103^+$ Trm cells relative to PBS-immunized mice (Fig. 7G, H).

Following Pa challenge, both HFD and LFD mice immunized with the L-PaF formulation displayed significantly reduced pulmonary bacterial burdens relative to PBS-immunized mice, regardless of FTY720 treatment (Fig. 7I, J). Thus, protection during this early (18-hour) secondary challenge was maintained despite blockade of circulating T-cell recruitment. This protective effect was consistent with the significant negative correlation observed between lung Trm frequency and pulmonary Pa burden in both the HFD and LFD cohorts (Fig. S6C), supporting an association between lung-resident memory T-cell abundance and early bacterial control. Collectively, these data indicate that circulating memory T cells are not required for early secondary protection in this model and are consistent with a dominant contribution of lung-resident immune mechanisms during this time frame.

Discussion

Given growing concerns about reduced vaccine efficacy in obese populations, particularly due to impaired immunoglobulin production, we investigated aspects of the immune system contributing to protection by vaccination in this group. Here we assessed our L-PaF vaccine o/w nanoemulsion formulation (± BECC438b) for efficacy in a DIO mouse model to determine how metabolic status influences immune response magnitude and quality in response to this L-PaF formulation. Ultimately, we wanted to determine whether nonhumoral immune components could compensate for impaired antibody production and confer protection in a metabolically compromised host. For comparative purposes, we included a low-fat diet (LFD) nutrient-matched cohort, and a group fed regular chow (RC). The RC was not nutrient-matched, but it was necessary to recapitulate prior work conducted on L-PaF efficacy in our laboratory.

The high-fat diet (HFD), LFD, and RC groups all displayed robust humoral and cellular immune responses. The HFD cohort, however, had both IgG and IgA titers that started to wane in the 28 days following the third and final vaccination. We also found that the functional quality of the antibody response in L-PaF/ME/BECC-immunized mice was significantly impaired in HFD-fed mice. Most notably, these mice exhibited lower titers for IgA, an antibody isotype implicated in mucosal defense against Pa. This finding is consistent with previous studies reporting obesity to impair mucosal immunity, likely through altered B-cell function and reduced isotype switching to IgA.[18,20,45] In addition to IgA, we observed reduced titers of IgG subclasses, IgG1 and IgG3, in HFD mice compared to their LFD and RC counterparts. This suggests a broader defect in class-switched antibody production. The transient rise in antibody titers that does occur in HFD mice may be attributed to an extrafollicular response rather than a GC-derived response, which might be due to increased frequency of plasmablasts and the corresponding lack of GC B-cell expansion in these mice.[46,47]

The lower IgA response observed in HFD-fed mice appears to be closely linked to impaired GC formation. We detected a significant reduction in both GC B cells and TFH cells in these mice, highlighting a disruption in key cellular interactions required for effective isotype switching and affinity maturation. Given the central role of GCs in generating high-affinity antibodies,[48,49] this deficiency suggests that obesity-associated metabolic dysfunction negatively impacts the formation and function of these critical immune structures. In contrast, LFD-fed mice not only preserved GC architecture but also demonstrated enhanced frequencies of GC B cells and TFH cells. In support of this observation, we found that the expression of CXCR5 on $CD4^+Bcl6^+$ and $CD4^+Bcl6^+Foxp3^+$ T cells, key markers guiding TFH/TFR migration to B-cell follicles, was markedly reduced in the HFD mice compared to their LFD counterparts. This reduction was paralleled by a failure to downregulate PD-1 upon immunization of HFD mice, a process that did occur in LFD mice. These findings align with previous studies indicating that PD-1 downregulation is critical for the upregulation of CXCR5, thereby facilitating TFH cell migration toward the B-cell zone and promoting optimal GC responses.[50,51] Although the precise mechanisms underlying this dysregulation remain unclear, our results point toward disrupted PD-1/CXCR5 signaling as a potential contributor to the impaired humoral response observed in obese mice. Further investigation is warranted to delineate the molecular pathways affected by metabolic dysfunction and to identify potential therapeutic targets that may restore effective GC responses in this vulnerable population.

The HFD mice also exhibited a decreased Brm response in the lungs, in contrast to the LFD mice, which maintained a robust population of lung Brm cells. Notably, immunized HFD mice showed no significant increase in Brm frequency, whereas a clear expansion was observed in their LFD counterparts. Given the importance of mucosal antibody responses in clearing pathogens such as Pa, and the critical role Brm cells play in this process, the reduced Brm response in HFD mice likely contributes to their impaired humoral immunity. This is supported by

the significantly lower IgG titers observed in the lung supernatants of HFD mice. Further analysis revealed reduced expression of CD80 and PDL2 on Brm cells from HFD mice compared to their LFD counterparts. Since both markers are associated with rapid differentiation of antibody-producing cells,[39] their decreased expression may underline the functional impairment of Brm cells in the HFD condition.

Interestingly, despite the impaired humoral responses observed in HFD-fed mice, we detected a notable expansion of lung tissue-resident memory T (Trm) cells following immunization with the L-PaF formulation. These cells are known to provide rapid, localized protection against respiratory pathogens and to contribute to early extra lymphoid recall responses.[52–54] Their presence across all immunized groups, and particularly their relative enrichment in HFD mice, suggests that Trm cells may partially compensate for deficient humoral immunity and contribute to the protection observed against Pa colonization in L-PaF–vaccinated mice. Importantly, our FTY720 studies demonstrate that early (18-hour) secondary protection is maintained in the absence of circulating T-cell recruitment, indicating that circulating memory T cells are not required during this early phase of the recall response. This finding highlights the critical role of localized immunity in controlling pulmonary infection and underscores the potential of Trm cells as a key effector arm of vaccine-induced protection, particularly in metabolically compromised hosts. Taken together, these results emphasize the importance of generating and sustaining lung Trm populations as a strategic feature of effective mucosal vaccines.

Our findings carry significant implications for vaccine development in metabolically compromised populations. As global obesity rates continue to rise, it becomes increasingly important to understand how excess adiposity and associated metabolic dysfunction impact vaccine performance. The impaired GC responses and disrupted mucosal immunity we observed in obese mice suggest that similar immune deficits may contribute to suboptimal vaccine efficacy in obese humans, particularly against pathogens like Pa that require strong mucosal immune defenses. On the other hand, the induction of lung Trm cells across dietary groups, especially in HFD-fed mice, highlights a promising avenue for overcoming impaired humoral responses for properly formulated vaccines. These findings suggest that optimizing vaccines to enhance tissue-localized T-cell responses could be particularly beneficial in individuals with metabolic dysfunction. Strategies such as the use of mucosal adjuvants or delivery platforms tailored to promote Trm cell formation may offer improved protection in this and perhaps other vulnerable populations. Although further studies are warranted to fully elucidate the role of lung Trm cells in the clearance of Pa in the absence of a robust Brm response and the establishment of long-term protection, identifying the molecular signals that drive their generation, maintenance, and functional activation during infection will be essential for guiding the development of next-generation mucosal vaccines.

Author contributions

S.B., D.R.H., and W.L.P. conceptualized the study. S.B. and D.R.H. conducted the primary in vitro and in vivo experiments and were responsible for data curation. Z.D. prepared the protein antigen and prepared the formulations. P.H., S.M., and T.L. contributed extensively to the experimental procedures. R.K.E. supplied BECC438b and contributed valuable insight during the later phases of the study. W.L.P. and W.D.P. provided strategic oversight and guidance throughout the project. The initial manuscript draft was written by S.B. and revised by D.R.H. Subsequent versions were critically reviewed and edited by W.L.P., W.D.P., and R.K.E.; W.D.P. offered substantive input on the final manuscript. W.L.P. secured the funding that supported this work.

Satabdi Biswas (Conceptualization [Equal], Data curation [Lead], Formal analysis [Lead], Investigation [Lead], Methodology [Lead], Software [Lead], Validation [Equal], Writing—original draft [Equal]), Debaki Ranjan Howlader (Conceptualization [Equal], Data curation [Supporting], Formal analysis [Supporting], Investigation [Supporting], Methodology [Supporting], Validation [Supporting], Writing—original draft [Equal]), Zackary Dietz (Methodology [Supporting]), Prolay Halder (Methodology [Supporting]), Suhrid Maiti (Methodology [Supporting]), Ti Lu (Methodology [Supporting]), Robert K. Ernst (Funding acquisition [Supporting], Resources [Supporting], Writing—review & editing [Supporting]), William D. Picking (Methodology [Supporting], Supervision [Supporting], Validation [Equal], Writing—review & editing [Equal]), and Wendy L. Picking (Conceptualization [Equal], Funding acquisition [Lead], Project administration [Lead], Supervision [Lead], Validation [Equal], Writing—review & editing [Equal])

Supplementary material

Supplementary material is available at *The Journal of Immunology* online.

Funding

This research was supported by the National Institute of Allergy and Infectious Diseases (NIAID), National Institutes of Health (NIH), U.S. Department of Health and Human Services, through a grant awarded to W.L.P. (R01AI169781), and a contract awarded to R.K.E. (HHSN272201800043C).

Conflicts of interest

W.L.P. and W.D.P. hold part ownership interests in Hafion, Inc. R.K.E. is a founder and serves as a scientific advisor and consultant for TollereBio Corporation, a Maryland-based biotechnology company that has licensed intellectual property from the University of Maryland–Baltimore related to the data presented in this study. All other authors declare no commercial or financial relationships that could be interpreted as potential conflicts of interest.

Data availability

All data are available from the corresponding author upon request.

References

1. Ogden CL, Carroll MD, Kit BK, Flegal KM. Prevalence of childhood and adult obesity in the United States, 2011–2012. JAMA. 2014;311:806–814.
2. Yu JY, Choi WJ, Lee HS, Lee JW. Relationship between inflammatory markers and visceral obesity in obese and overweight Korean adults: an observational study. Medicine (Baltimore). 2019;98:e14740.
3. Huizinga GP, Singer BH, Singer K. The collision of meta-inflammation and SARS-CoV-2 pandemic infection. Endocrinology. 2020;161:bqaa154.
4. Entrup GP et al. Obesity inhibits alveolar macrophage responses to pseudomonas aeruginosa pneumonia via upregulation of prostaglandin E2 in male, but not female, mice. J Immunol. 2024;213:317–327.
5. Mancuso P et al. Diet-induced obesity in mice impairs host defense against Klebsiella pneumonia in vivo and glucose transport and bactericidal functions in neutrophils in vitro. Am J Physiol Lung Cell Mol Physiol. 2022;322:L116–L128.
6. Ho JSY, Fernando DI, Chan MY, Sia CH. Obesity in COVID-19: a systematic review and meta-analysis. Ann Acad Med Singap. 2020;49:996–1008.
7. Morgan OW et al. Morbid obesity as a risk factor for hospitalization and death due to 2009 pandemic influenza A(H1N1) disease. PLoS One. 2010;5:e9694.
8. Pugliese G et al. Obesity and infectious diseases: pathophysiology and epidemiology of a double pandemic condition. Int J Obesity. 2022;46:449–465.
9. Mancuso P. Obesity and respiratory infections: does excess adiposity weigh down host defense? Pulm Pharmacol Ther. 2013;26:412–419.
10. Torres A et al. Pneumonia. Nat Rev Dis Primers. 2021;7:25.
11. World Health Organization. WHO bacterial priority pathogens list 2024: bacterial pathogens of public health importance, to guide research, development, and strategies to prevent and control antimicrobial resistance. 1st ed. World Health Organization; 2024. https://www.who.int/publications/i/item/9789240093461
12. Döring G, Pier GB. Vaccines and immunotherapy against *Pseudomonas aeruginosa*. Vaccine. 2008;26:1011–1024.
13. Reynolds D, Kollef M. The epidemiology and pathogenesis and treatment of *Pseudomonas aeruginosa* infections: an update. Drugs. 2021;81:2117–2131.
14. Centers for Disease Control and Prevention. 2019 antibiotic resistance threats report. Centers for Disease Control and Prevention; 2022. https://www.cdc.gov/antimicrobial-resistance/data-research/threats/index.html
15. Hamson E et al. Impact of pandemics and disruptions to vaccination on infectious diseases epidemiology past and present. Hum Vaccin Immunother. 2023;19:2219577.
16. Montero DA et al. Two centuries of vaccination: historical and conceptual approach and future perspectives. Front Public Health. 2024;11:1326154.
17. Sheridan PA et al. Obesity is associated with impaired immune response to influenza vaccination in humans. Int J Obes (Lond). 2012;36:1072–1077.
18. Chauvin C, Retnakumar SV, Bayry J. Obesity negatively impacts maintenance of antibody response to COVID-19 vaccines. Cell Rep Med. 2023;4:101117.
19. Karlsson EA et al. Obesity outweighs protection conferred by adjuvanted influenza vaccination. mBio. 2016;7:e00144-16.
20. Painter SD, Ovsyannikova IG, Poland GA. The weight of obesity on the human immune response to vaccination. Vaccine. 2015;33:4422–4429.
21. Eliakim A, Schwindt C, Zaldivar F, Casali P, Cooper DM. Reduced tetanus antibody titers in overweight children. Autoimmunity. 2006;39:137–141.
22. Das S et al. Development of a broadly protective, self-adjuvanting subunit vaccine to prevent infections by *Pseudomonas aeruginosa*. Front Immunol. 2020;11:583008.
23. Howlader DR et al. Effect of two unique nanoparticle formulations on the efficacy of a broadly protective vaccine against *Pseudomonas aeruginosa*. Front Pharmacol. 2021;12:706157.
24. Gregg KA et al. Rationally designed TLR4 ligands for vaccine adjuvant discovery. mBio. 2017;8:e00492-17.
25. Howlader DR et al. A protein subunit vaccine elicits a balanced immune response that protects against *Pseudomonas* pulmonary infection. NPJ Vaccines. 2023;8:37.
26. Howlader DR et al. Development of a nano-emulsion based multivalent protein subunit vaccine against *Pseudomonas aeruginosa*. Front Immunol. 2024;15:1372349.
27. Baruah N et al. Development of a self-adjuvanting, cross-protective, stable intranasal recombinant vaccine for shigellosis. ACS Infect Dis. 2021;7:3182–3196.
28. Wang Y et al. Development of a chimeric vaccine against *Pseudomonas aeruginosa* based on the Th17-stimulating epitopes of PcrV and AmpC. Front Immunol. 2020;11:601601.
29. Schaefers MM et al. PLGA-encapsulation of the *Pseudomonas aeruginosa* PopB vaccine antigen improves Th17 responses and confers protection against experimental acute pneumonia. Vaccine. 2018;36:6926–6932.
30. Gregg KA et al. A lipid A-based TLR4 mimetic effectively adjuvants a *Yersinia pestis* rF-V1 subunit vaccine in a murine challenge model. Vaccine. 2018;36:4023–4031.
31. Yang Y, Smith DL Jr, Keating KD, Allison DB, Nagy TR. Variations in body weight, food intake and body composition after long-term high-fat diet feeding in C57BL/6J mice. Obesity (Silver Spring). 2014;22:2147–2155.
32. Scott P. IL-12: initiation cytokine for cell-mediated immunity. Science. 1993;260:496–497.
33. Gilmour BC, Corthay A, Øynebråten I. High production of IL-12 by human dendritic cells stimulated with combinations of pattern-recognition receptor agonists. NPJ Vaccines. 2024;9:83.
34. Trinchieri G. Interleukin-12 and the regulation of innate resistance and adaptive immunity. Nat Rev Immunol. 2003;3:133–146.
35. Watford WT, Moriguchi M, Morinobu A, O'Shea JJ. The biology of IL-12: coordinating innate and adaptive immune responses. Cytokine Growth Factor Rev. 2003;14:361–368.
36. Bain CC, Macdonald AS. The impact of the lung environment on macrophage development, activation and function:

diversity in the face of adversity. Mucosal Immunol. 2022; 15:223–234.
37. Kawasaki T et al. Alveolar macrophages instruct CD8(+) T cell expansion by antigen cross-presentation in lung. Cell Rep. 2022;41:111828.
38. Kim Y-J, Choi J, Choi YS. Transcriptional regulation of Tfh dynamics and the formation of immunological synapses. Exp Mol Med. 2024;56:1365–1372.
39. Zuccarino-Catania GV et al. CD80 and PD-L2 define functionally distinct memory B cell subsets that are independent of antibody isotype. Nat Immunol. 2014;15:631–637.
40. Hondowicz BD, Kim KS, Ruterbusch MJ, Keitany GJ, Pepper M. IL-2 is required for the generation of viral-specific CD4(+) Th1 tissue-resident memory cells and B cells are essential for maintenance in the lung. Eur J Immunol. 2018;48:80–86.
41. Gebhardt T et al. Memory T cells in nonlymphoid tissue that provide enhanced local immunity during infection with herpes simplex virus. Nat Immunol. 2009;10:524–530.
42. Chiba K. FTY720, a new class of immunomodulator, inhibits lymphocyte egress from secondary lymphoid tissues and thymus by agonistic activity at sphingosine 1-phosphate receptors. Pharmacol Ther. 2005;108:308–319.
43. Brinkmann V et al. Fingolimod (FTY720): discovery and development of an oral drug to treat multiple sclerosis. Nat Rev Drug Discov. 2010;9:883–897.
44. Youngblood B, Hale JS, Ahmed R. T-cell memory differentiation: insights from transcriptional signatures and epigenetics. Immunology. 2013;139:277–284.
45. Frasca D et al. The majority of SARS-CoV-2–specific antibodies in COVID-19 patients with obesity are autoimmune and not neutralizing. Int J Obes (Lond). 2022;46:427–432.
46. Oleinika K, Slisere B, Catalán D, Rosser EC. B cell contribution to immunometabolic dysfunction and impaired immune responses in obesity. Clin Exp Immunol. 2022;210:263–272.
47. Elsner RA, Shlomchik MJ. Germinal center and extrafollicular B cell responses in vaccination, immunity, and autoimmunity. Immunity 2020;53:1136–1150.
48. Olatunde AC, Hale JS, Lamb TJ. Cytokine-skewed Tfh cells: functional consequences for B cell help. Trends Immunol. 2021;42:536–550.
49. Nutt SL, Tarlinton DM. Germinal center B and follicular helper T cells: siblings, cousins or just good friends? Nat Immunol. 2011;12:472–477.
50. Shi J et al. PD-1 controls follicular T helper cell positioning and function. Immunity. 2018;49:264–274.e264.
51. Vanderleyden I et al. Follicular regulatory T cells can access the germinal center independently of CXCR5. Cell Rep. 2020; 30:611–619.e614.
52. Finn CM et al. Airway-resident memory CD4 T cell activation accelerates antigen presentation and T cell priming in draining lymph nodes. JCI Insight. 2024;10:e182615.
53. Zens KD, Chen JK, Farber DL. Vaccine-generated lung tissue-resident memory T cells provide heterosubtypic protection to influenza infection. JCI Insight. 2016;1:e85832.
54. Fumagalli V et al. Antibody-independent protection against heterologous SARS-CoV-2 challenge conferred by prior infection or vaccination. Nat Immunol. 2024;25:633–643.

The Journal of Immunology, 2026, 215, 1–16
https://doi.org/10.1093/jimmun/vkag052
Research Article